Estimation of evaporation over the upper Blue Nile basin by combining observations from satellites and river flow gauges

AGU PUBLICATIONS

Water Resources Research

RESEARCH ARTICLE

10.1002/2015WR017251

Estimation of evaporation over the upper Blue Nile basin by combining observations from satellites and river flow gauges

Mariam M. Allam[1], Anjuli Jain Figueroa[1], Dennis B. McLaughlin[1], and Elfatih A. B. Eltahir[1]

[1]Ralph M. Parsons Laboratory, Massachusetts Institute of Technology, Cambridge, Massachusetts, USA

Key Points:
- Global evaporation data sets underestimate evaporation over the UBN basin
- We estimate an annual ET over the UBN basin of about 2.55 mm per day
- Natural vegetation is a water-efficient system in the western side of the basin

Correspondence to:
M. Allam, Ćmallam@mit.edu

Citation:
Allam, M. M., A. Jain Figueroa, D. B. McLaughlin, and E. A. B. Eltahir (2016), Estimation of evaporation over the upper Blue Nile basin by combining observations from satellites and river flow gauges, *Water Resour. Res.*, *52*, doi:10.1002/2015WR017251.

Received 17 MAR 2015
Accepted 2 JAN 2016
Accepted article online 7 JAN 2016

Abstract Reliable estimates of regional evapotranspiration are necessary to improve water resources management and planning. However, direct measurements of evaporation are expensive and difficult to obtain. Some of the difficulties are illustrated in a comparison of several satellite-based estimates of evapotranspiration for the Upper Blue Nile (UBN) basin in Ethiopia. These estimates disagree both temporally and spatially. All the available data products underestimate evapotranspiration leading to basin-scale mass balance errors on the order of 35 percent of the mean annual rainfall. This paper presents a methodology that combines satellite observations of rainfall, terrestrial water storage as well as river-flow gauge measurements to estimate actual evapotranspiration over the UBN basin. The estimates derived from these inputs are constrained using a one-layer soil water balance and routing model. Our results describe physically consistent long-term spatial and temporal distributions of key hydrologic variables, including rainfall, evapotranspiration, and river-flow. We estimate an annual evapotranspiration over the UBN basin of about 2.55 mm per day. Spatial and temporal evapotranspiration trends are revealed by dividing the basin into smaller subbasins. The methodology described here is applicable to other basins with limited observational coverage that are facing similar future challenges of water scarcity and climate change.

1. Introduction

The Nile River basin is shared by eleven countries, five of which are relatively underdeveloped. About 370 million people rely on the Nile's water, and the basin's population is projected to continue growing significantly which will intensify water scarcity problems in the region. With over two thirds of the basin's agriculture being subsistence rain-fed farming and the low rate of application of fertilizers, the agricultural yields in the basin are very low compared to the average global yields. The Nile basin has large agricultural and hydropower potentials that have not yet been tapped, but with the high dependence of its riparian countries on its water any development project can be a source of conflict in the region. A major recent conflict involves three countries: Egypt, Ethiopia, and Sudan. These countries share the Blue Nile basin, which contributes over 60 percent of the flow measured at Aswan. Since the announcement of the Grand Ethiopian Renaissance Dam (GERD) at the outlet of the Upper Blue Nile (UBN) basin, a conflict over this dam has been escalating between Egypt and Ethiopia. A lack of adequate data and comprehensive knowledge of key hydrologic variables has only contributed to worsening the conflict with each side taking positions based on inadequate information.

A reanalysis system produces data sets through a frozen data assimilation scheme and model which merges available observations (irregular in space and time) with model forecast to generate uniform gridded data. There are several atmospheric reanalysis data sets available such as the Japanese 25 year reanalysis data (JRA-25) which was released in March 2006 [*Onogi et al.*, 2005, 2007]; the 40 year European Centre for Medium-Range Weather Forecasts (ECMWF) Re-Analysis data (ERA-40) available for the period 1979–2002 [*Uppala et al.*, 2005]; the National Centers for Atmospheric Research—Department of Energy 2nd reanalysis data (NCEP-DOE R2) [*Kanamitsu et al.*, 2002]; the ERA-Interim reanalysis data also produced by ECMWF available for the period 1989–current [*Simmons et al.*, 2007; *Uppala et al.*, 2008]; the NCEP-CFSR released in 2010 [*Saha et al.*, 2010] and the modern-era reanalysis (MERRA) available for the period 1979–current [*Rienecker et al.*, 2011]. The reanalysis products have been proven useful in driving land surface models, studying the climate system, validating General Circulation Models (GCMs) and providing boundary conditions for regional modeling [*Decker et al.*, 2012]. However, they should be used with appropriate care since their

reliability varies depending on the location, time, and variable considered since they are observation driven and the changing mix of observations ingested to the model at each time step can introduce artificial variability and false trends. *Siam et al*. [2013] have compared the hydrologic cycle of GCMs and reanalysis products over the Congo and the upper Blue Nile basins. They found that the ERA-40 and the NCEP-NCAR do not satisfy the atmospheric and soil water balances and their simulated seasonal cycles do not match observations. ERA-Interim was found to have a better performance regarding balancing the water budget and representing the seasonal cycle of the hydrological variable, however it overestimates the hydrological variables compared to observations.

Remote sensing and global satellite data have become readily available sources for testing models of land and water resources. It would seem that the readily available remote sensing data sets can be used to determine regional water budgets accurately. However, different data sets come from different instruments with different accuracies, resolution, and coverage, using different algorithms. These differences lead to significant discrepancies and inconsistencies between available data sets for key variables such as precipitation and evapotranspiration. There have been several attempts to estimate the terrestrial water budget at large scales using remote sensing and satellite data. *Sahoo et al*. [2011] assessed the terrestrial water budgets using remote sensing data sets over 20 large global river basins and significant uncertainties were traced to the precipitation data sets. *Sheffield et al*. [2009] attempted to close the water budget for the Mississippi River basin and found significant errors that were larger than the observed streamflow even after removing systematic biases in the remote sensing estimates of precipitation and evaporation. *Gao et al*. [2010] estimated the water budget of major U.S. river basins using satellite data and evaluated them using gridded precipitation observation and the Variable Infiltration Capacity (VIC) model evaporation and water storage. This study concluded that water budget closure at the scale of large continental river basins using satellite data alone is not possible, and the largest sources of nonclosure errors are precipitation and evaporation. *Pan and Wood* [2006] have proposed a constrained ensemble Kalman-filter data assimilation procedure to merge observations and Variable Infiltration Capacity (VIC) model estimates and assure closure of the water balance. *Pan et al*. [2012] have merged several satellite and reanalysis data in a data assimilation model to estimate the long-term terrestrial water budget for major global river basins. They concluded that the error analysis for each water budget variable is challenging at the global scale and that the error analysis for evapotranspiration lack supportive quantitative analysis and may not hold for specific locations.

Here the annual water budget of the UBN basin was investigated using the TRMM 3B43 v7 annual precipitation depth of about (1359 mm), the WM annual actual evapotranspiration of about (639 mm), and the Flow Gauge measurements at Diem station the outlet of the UBN basin of about (276 mm). The water budget closure error was found to be 444 mm which is about 35 percent of the annual rainfall falling over the UBN basin.

Readily available global data sets that describe evapotranspiration based on satellite observations over the UBN basin do not agree on the spatial or the temporal distributions, as shown in Figures 1 and 2. Evapotranspiration is an important component of the water budget which influences the planning of agricultural development projects and cropping strategies and the releases from hydropower dams. The objective of this paper is to develop a more accurate self-consistent picture of the UBN basin's hydrology to aid the decision-making process for developing the basin.

2. The Upper Blue Nile Basin Description

The UBN basin also known as the Abbay basin is located in the Ethiopian highlands with a drainage area of about 176, 000 km^2 (Table 1). It extends from 7°40′ to 12°5′ N and from 34°25′ to 39°49′ E (Figure 3). The river extends from its origin at Lake Tana to the Sudanese border at Diem with a contribution of 60 percent of the Nile flow measured at Aswan. The basin's climate varies from humid to semiarid. The annual precipitation increases from northeast to southwest and ranges from 1200 to 1600 mm as shown in Figure 4 [*Conway*, 1997, 2000; *Tafesse*, 2001; *Kim et al*., 2008]. Most of the precipitation occurs in the wet season called locally Kiremt (June–September) and less precipitation occurs in the dry and mild seasons known locally as Bega (October–February) and Belg (February–May). The interannual variability of the upper Blue Nile precipitation in the wet season is correlated with El-Nino southern oscillations in which the rainfall tend to be high during La-Nina events and low during El-Nino events [*Eltahir*, 1996; *Siam and Eltahir*, 2015; *Siam et al*.,

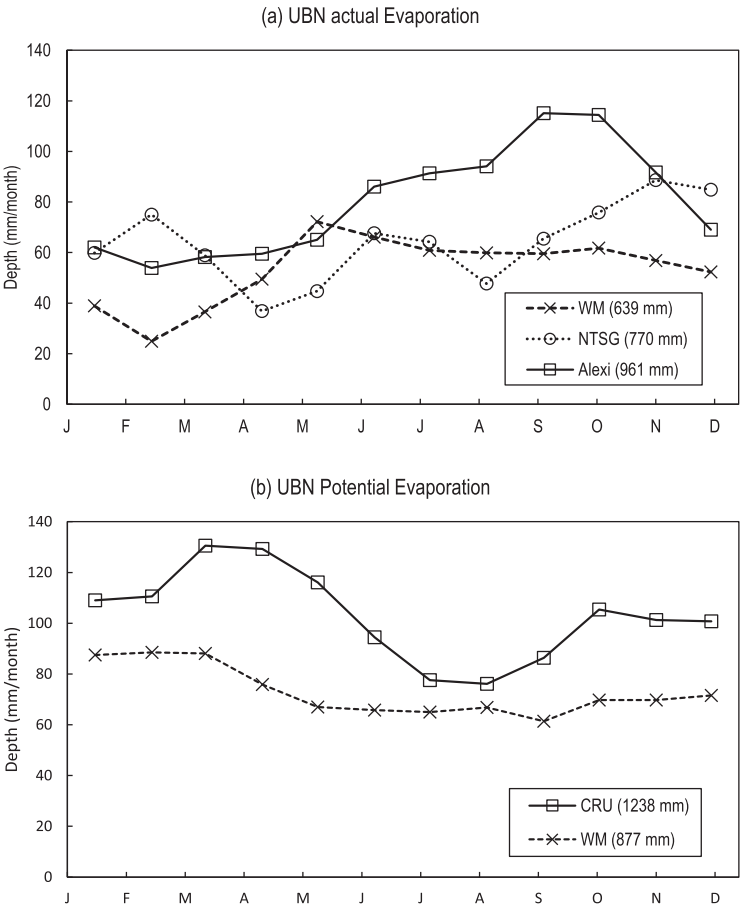

Figure 1. (a) Comparison of the spatial long-term average actual evapotranspiration for the ALEXI, NTSG, and WM data sets over the UBN basin for the period 2002–2013. (b) Comparison of the CRU and WM long-term spatial average potential evaporation over the UBN basin for the period 2002–2013.

2014]. The mean annual temperature is about 18.5°C with a seasonal variation of less than 2°C [*Kim et al.*, 2008] and the annual potential evapotranspiration is estimated to be about 1100 mm [*Gamachu*, 1977; *Kim et al.*, 2008]. The eastern part of the basin has the highest elevation reaching 4000 m above mean sea level and decreasing gradually toward the western outlet of the basin where the elevation is approximately 500 m above mean sea level as shown in Figure 3.

3. Data Assimilation Procedure

3.1. General Approach

Our approach for characterizing the UBN hydrology is to extract the greatest possible information from available data using data assimilation techniques McLaughlin [1995]; Houser et al. [1998]; Pan and Wood [2006]; Pan et. al. [2012]. We treat the hydrological fluxes and states within the UBN basin as uncertain variables that are estimated from imperfect measurements while honoring physical constraints. The estimation process is posed as an optimization problem. The objective is to minimize the weighted mean-squared error between estimates and measurements of observed hydrologic variables. The minimization process is constrained by mass and energy balance relationships and relevant hydrologic thresholds. The variables to be estimated (the decision variables in the optimization problem) are: precipitation, evapotranspiration, potential evaporation, flow-routing, and water storage within the basin. The result of the data assimilation process is a set of spatially distributed hydrologic flux and storage estimates that are physically consistent as well as compatible with observations. The estimates can then be used for planning and management studies.

3.2. Optimization Objective Function

The objective of the data assimilation optimization problem is the minimization of the weighted squared deviations between the estimated and measured values of each hydrologic variable. The least-squared error objective function is written as:

$$\text{Min}\left[\begin{array}{c}\sum_m\sum_n w_P\delta^2_{P_{n,m}}+\sum_m\sum_n w_{PET}\delta^2_{PET_{n,m}}+\sum_g\sum_m w_R\delta^2_{R_{m,g}}\\+\sum_m\sum_n w_{ET_{noncrop}}\delta^2_{ET_{noncrop\,n,m}}+\sum_m\sum_n w_{ET_{crop}}\delta^2_{ET_{crop\,n,m}}+\sum_m w_S\delta^2_{S_m}\end{array}\right] \quad (1)$$

Where the normalized differences between measurements and estimates are defined as follows:

$$\delta_{P_{n,m}}:\ \text{Pixel precipitation misfit}=\frac{1}{P}\left[\boldsymbol{P_{n,m}}-P'_{n,m}\right] \quad (2)$$

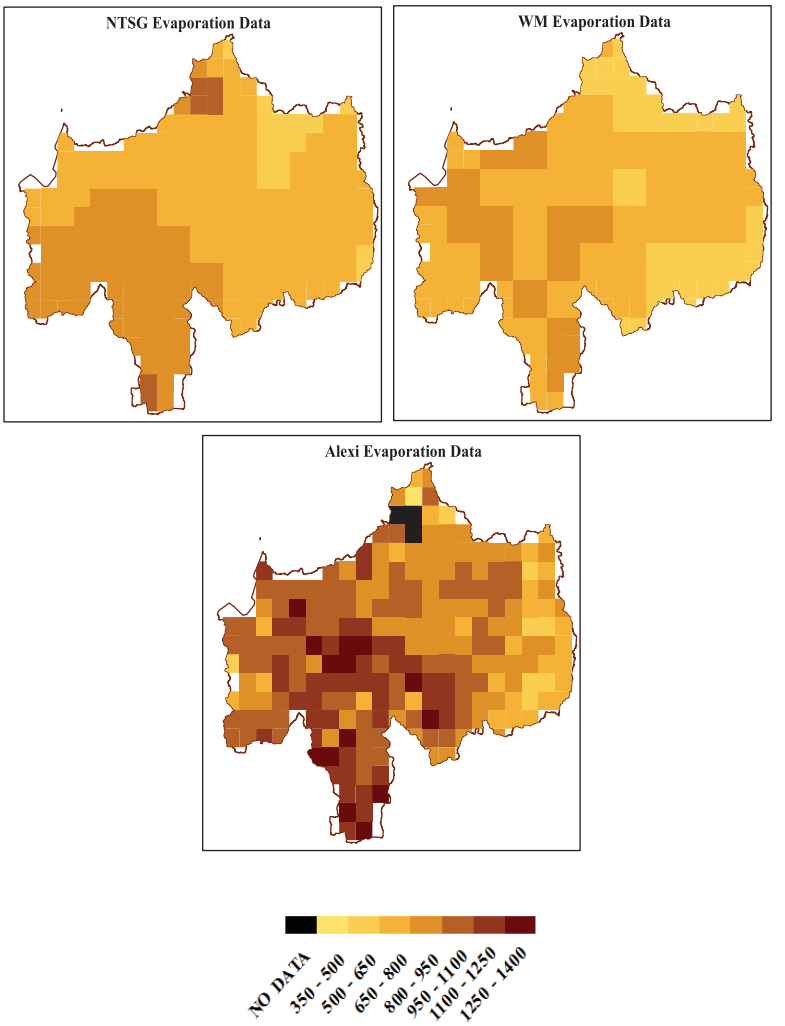

Figure 2. A comparison between the spatial distribution of the long-term average annual actual evapotranspiration depth of the NTSG, WM, and ALEXI data sets for the period 2002–2013.

$$\delta_{PET_{n,m}}: \text{Pixel Potential Evapotranspiration misfit} = \frac{1}{\bar{P}}\left[\boldsymbol{PET_{n,m}} - PET'_{n,m}\right] \tag{3}$$

$$\delta_{R_{n,m}}: \text{Gauge Runoff misfit} = \frac{1}{\bar{R}}\left[\boldsymbol{R_{m,g}} - R_{m,g}\right] \tag{4}$$

$$\delta_{ET_{noncrop_{n,m}}}: \text{Pixel non-crop ET misfit} = \frac{1}{\overline{ET_{noncrop}}}\left[\boldsymbol{ET_{noncrop_{n,m}}} - ET'_{noncrop_{n,m}}\right] \tag{5}$$

$$\delta_{ET_{crop_{n,m}}}: \text{Pixel crop ET misfit} = \frac{1}{\overline{ET_{crop}}}\left[\boldsymbol{ET_{crop_{n,m}}} - ET'_{crop_{n,m}}\right] \tag{6}$$

$$\delta_{S_{n,m}}: \text{UBN basin storage misfit} = \frac{1}{\bar{S}}\left[\boldsymbol{S_m} - S'_m\right] \tag{7}$$

Normalization factors are used to give the objective function terms a dimensionless nature. These factors are calculated as the averages of the corresponding measurements over time and space (indicated by overbars).

The weights assigned to the hydrologic budget terms such as w_P, w_{PET}, w_R, $w_{ET_{noncrop}}$, $w_{ET_{crop}}$, and w_S are calculated to be inversely proportional to the possible errors in the data sets inferred from: (1) the error variance of the data set used as input to the model for each hydrologic variable, (2) the variation across different

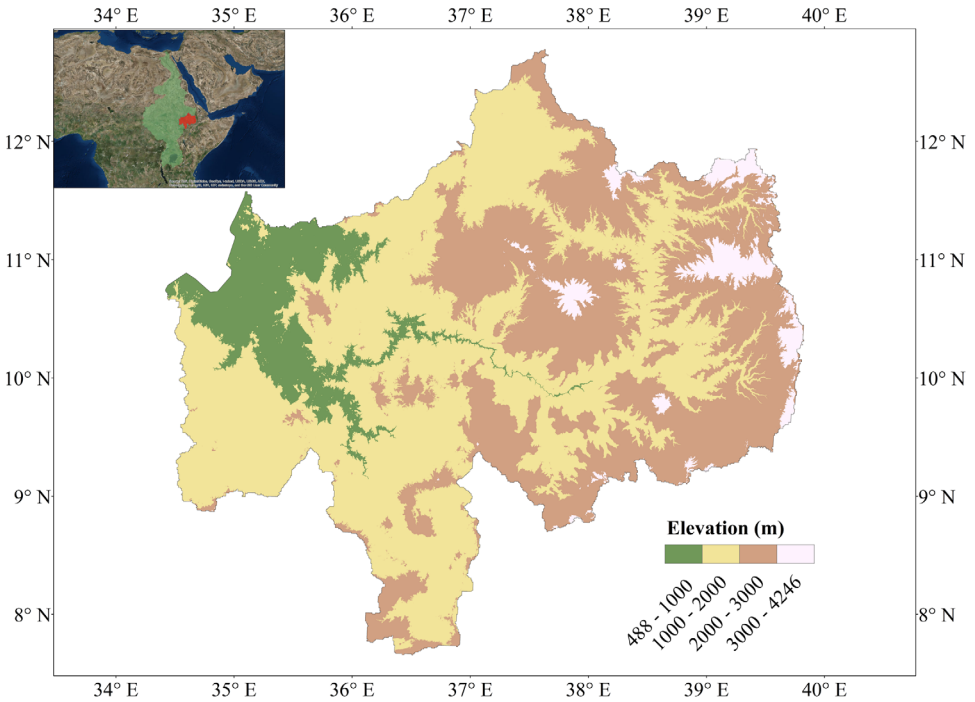

Figure 3. Upper Blue Nile Basin within the Nile Basin in Africa. Inset shows UBN basin topography.

data sets examined for each hydrologic variable. For instance, the expected errors in the runoff and precipitation data sets were found to be about 10 and 50 percent.

In order to check the sensitivity of the data assimilation procedure to the weights, the weights were varied by factors of 0.1, 0.5, 2, and 10. The resulting assimilated hydrologic variables changed only by 0.5 and 5%, respectively.

3.3. Constraints

The least-squares data assimilation procedure is based on a set of constraints that describe physical relationships among uncertain hydrologic variables. These equations collectively define an UBN river basin model. The model is formulated on a regular grid of quarter degree (~25 km) pixels and describes temporal changes over a typical year, using a monthly time step to investigate the long-term monthly averaged variability in the UBN basin hydrology. The model can be easily extended in the future to investigate interannual variability in the hydrological time series.

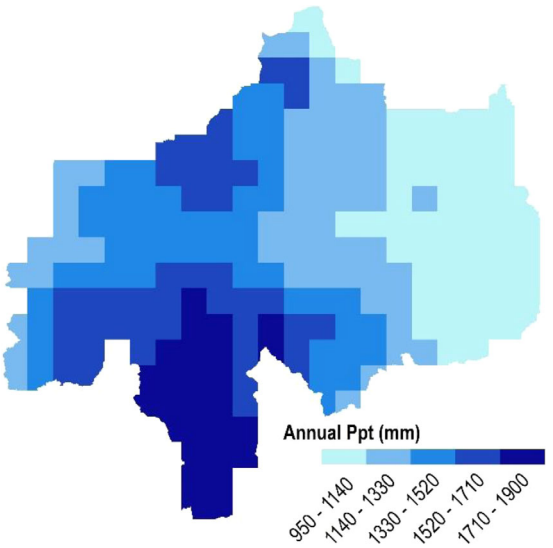

Figure 4. A map of the TRMM annual precipitation depth over the upper Blue Nile basin for the period 2002–2013.

The water budget (or mass balance) equation for each pixel is:

$$\Delta S_{n,m} = S_{n,m+1} - S_{n,m} = Qin_{n,m} + P_{n,m} - ET_{n,m} - Qout_{n,m} \quad (8)$$

where $\Delta S_{n,m}$ is the change in the monthly storage of pixel n (km^3/month), Q_{in} is the flow into the pixel from tributary pixels contributing into it, and Q_{out} is the outflow from the pixel as shown in the schematic diagram in Figure 5, $P_{n,m}$ is the pixel monthly precipitation (km^3/month) and $ET_{n,m}$ is the pixel monthly evapotranspiration (km^3/month). The inflow to pixel *n* is the sum of all contributions from upstream pixels:

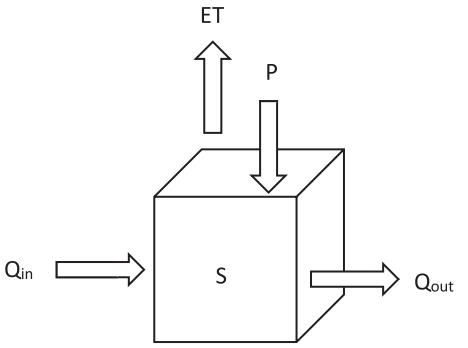

Figure 5. A schematic diagram of a typical grid cell with hydrologic variables used in the data assimilation procedure.

Table 1. Summary of the UBN Basin Characteristics

Characteristic	
Area (km^2)	176,000
Mean annual precipitation (mm d^{-1})	1224
Mean annual streamflow (km^3)	46

$$\boldsymbol{Qin}_{n,m} = \sum_{trib}\left(\Delta t\left(\boldsymbol{P}_{n,m} - \boldsymbol{ET}_{n,m} - \Delta \boldsymbol{S}_{n,m}\right)\right) \quad (9)$$

The storage in each pixel is limited by the soil water holding capacity of an assumed 1.5 m depth root zone. If the storage exceeds the capacity the excess water contributes to runoff towards a downstream pixel.

$$\boldsymbol{S}_{n,m} \leq S_{threshold\,n} \quad (10)$$

Similarly the change in storage in each pixel is constrained by the infiltration capacity of the soil.

$$\Delta S_{\min} \leq \Delta \boldsymbol{S}_{n,m} \leq \Delta S_{\max} \quad (11)$$

where $S_{threshold}$ is the storage water holding capacity in pixel n (km^3) and $\Delta S_{\min}$&$\Delta S_{\max}$ are the infiltration and exfiltration capacity rates of the basin's soil.

The flow from the river basin outlet is the outflow from the most downstream pixel which is calculated through summing the pixel hydrologic fluxes in the whole basin contributing to the most downstream pixel.

$$\boldsymbol{R}_{m,g} = \boldsymbol{Q}_{out_{g,m}} \quad (12)$$

Where $\boldsymbol{R}_{m,g}$ is the UBN basin monthly run-off (km^3/month) and $\boldsymbol{Q}_{out_{g,m}}$ is the monthly outflow from the pixel at the location of gauge g (km^3/month).

Additional constraints are used to divide evaporation into three components: evaporation from water bodies $\left(\boldsymbol{ET}_{lake_{n,m}}\right)$, crop evapotranspiration $\left(\boldsymbol{ET}_{crop_{n,m}}\right)$, and evaporation from natural vegetation and soils $\left(\boldsymbol{ET}_{non-crop_{n,m}}\right)$ all represented as follows:

$$\boldsymbol{ET}_{n,m} = \boldsymbol{ET}_{crop_{n,m}} + \boldsymbol{ET}_{non-crop_{n,m}} + \boldsymbol{ET}_{lake_{n,m}} \quad (13)$$

$$\boldsymbol{ET}_{crop_{n,m}} = K_{cropgen_{n,m}}\, \boldsymbol{PET}_{n,m}\left(A_{crop_n}/A_n\right) \quad (14)$$

$$\boldsymbol{ET}_{lake_{n,m}} = \boldsymbol{PET}_{n,m} \quad (15)$$

where $K_{cropgen_{n,m}}$ is a generalized crop factor calculated based on the cropping patterns in the UBN basin, $\boldsymbol{PET}_{n,m}$ is the monthly potential evaporation from pixel n (km^3/month), and (A_{crop_n}/A_n) is the crop area fraction of pixel n.

Evapotranspiration is constrained to be no greater than net radiation minus the sensible and ground heat fluxes heat. This is represented in our model as:

$$\boldsymbol{ET}_{n,m} \leq \frac{R_{net\,n,m}}{\lambda CF} + \boldsymbol{C}\Delta T_{n,m} \quad (16)$$

where $R_{net\,n,m}$ is the monthly available net radiation for pixel n (W/m^2), λ is the latent heat of vaporization (kJ/kg), CF is a unit conversion factor, C is a constant parameter to be estimated by the model that accounts for the sensible and ground heat fluxes and $\Delta T_{n,m}$ is the monthly change in temperature at pixel n. In addition to the above constraints, all variables are constrained to be nonnegative. The least-squares data assimilation problem with these mass and energy balance constraints have a unique optimum solution because it has a convex quadratic objective and its constraints are all linear [*Markowitz*, 1956].

4. Data

Table 2 summarizes the data sets used as inputs to the objective function and the constraints equations. Here we examine differences between the several data sets examined over the UBN basin and explain why we chose particular data sets for the UBN basin analysis.

Table 2. Summary of the Data Sets Considered and Used in the Data Assimilation Procedure

Data	Source (Abbreviation)	Spatial Resolution	Data Citation
River Flow Routing			
Topography data	SRTM	90 m	USGS, 2004
Flow direction data	NTSG-DRT	0.25°	*Wu et al.* [2011]
Crop data			
Crop coefficients			
Crop maps	Cropland and pasture data	0.5°	Ramankutty and Foley [1999]
Crop patterns	Major crops	0.5°	*Ramankutty and Foley* [1998]; Leff et al. [2004]
Temperature	CRU TS3	0.5°	
Precipitation	CRU TS3	0.5°	*Mitchel and Jones* [2005]
	TRMM	0.25°	*Huffman et al.* [2007]
	GPCP	2.5°	*Adler et al.* [2003]
Evapotranspiration	WM	0.5°	*Willmott and Matsuura* [2000]
	NTSG	0.5°	*Zhang et al.* [2009]; Zhang et al. [2010]
	ALEXI	0.027°	*Anderson et al.* [2007a, 2007b,]
Potential evaporation	WM	0.5°	*Willmott and Matsuura* [2000]
	CRU TS3	0.5°	*Mitchell and Jones* [2005]
Soil moisture	GRACE	1°	*Chambers et al.* [2006]
	CPC	0.5°	*van den Dool et al.* [2003]
	ESA	0.25°	*Liu et al.* [2012];
Soil water holding capacity	HWSD	1 km	*Nachtergaele* [1999]; FAO [2012]
Radiation data	NASA-SRB	1°	*Darnell et al.* [1996]; *Gupta et al.* [1999]

4.1. Objective Function Inputs

The data assimilation procedure adjusts estimates of hydrologic variables to obtain the best physically consistent fit to available measurements. In the UBN application, the measurements considered are satellite observations of rainfall, evapotranspiration, and terrestrial water storage as well as river flow gauge measurements. Since the final results depend significantly on the data set selected and on the amount of adjustment required to fit the data several global data sets were screened to choose the most appropriate inputs for the UBN. The following paragraphs summarize the results of the screening process:

4.1.1. Precipitation Data

The precipitation data sets examined and compared over the upper Blue Nile basin are: the Climatic Research Unit (CRU) [*Mitchell and Jones*, 2005], the Tropical Rainfall Measuring Mission (TRMM) [*Huffman et al.*, 2007], and the Global Precipitation Climatology Project (GPCP) [*Adler et al.*, 2003]. In general the three data sets agree on the temporal distribution of rainfall over the basin, and the difference between their estimates of annual rainfall is less than 5 percent as shown in Figure 6. Accordingly, the TRMM data set was chosen because of its higher resolution.

4.1.2. Potential Evaporation

The potential evaporation sources examined are: the Climatic Research Unit (CRU) data set [*Mitchell and Jones*, 2005] and the Willmot Matsuura (WM) data set [*Willmott and Matsuura*, 2000], both shown in Figure 1. It was found that WM generally underestimates the potential evaporation over the UBN basin when compared to previous studies [*Conway*, 1997; *Tekleab et al.*, 2011]. Consequently, the CRU data set was selected for the data assimilation procedure.

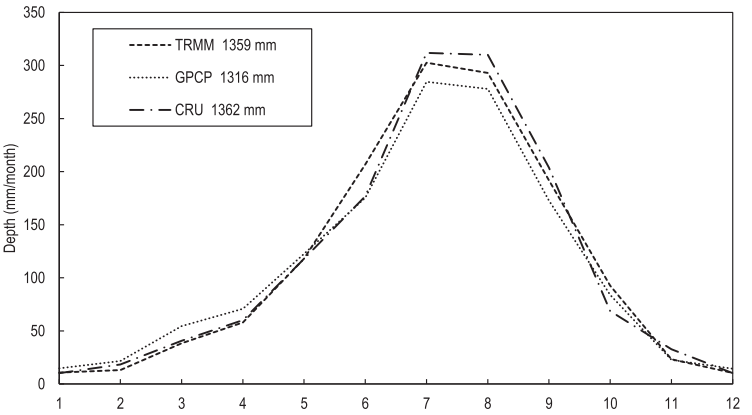

Figure 6. Comparison of the temporal distributions of TRMM, CRU, and GPCP precipitation over the UBN basin for the period 2002–2013.

4.1.3. River Flow Data

Flow data from nine river flow gauges (Diem, Megech, Ribb, Gumera, Bahir Dar, Gilgel Aba, Mendaya, Kardobi, and Kessie) are used in the data assimilation procedure to improve the river flow routing. The stations locations' and names are shown in Figure 7.

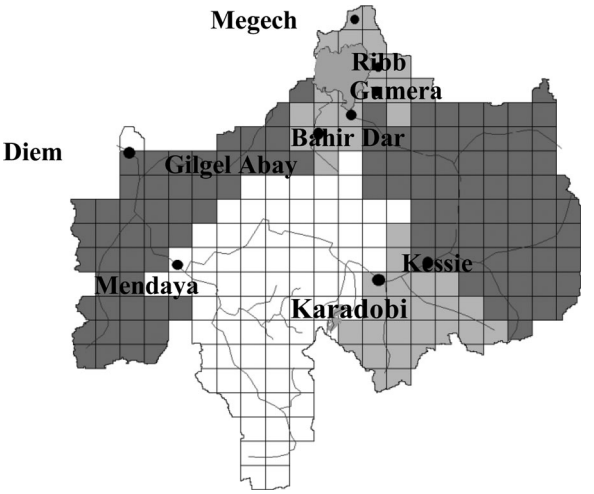

Figure 7. A map of the UBN basin showing the flow gauge stations locations.

4.1.4. Actual Evapotranspiration Data

Various evaporation data sets were examined over the upper Blue Nile basin and were all found to underestimate actual evaporation, compared to estimates obtained from water budget calculations, and to give different spatial and temporal distributions, as shown in Figures 1 and 2.The data sets investigated were: the WM data [*Willmott and Matsuura*, 2000], the Numerical Terradynamic Simulation Group (NTSG) data [*Zhang et al*., 2009], and The Atmosphere-Land exchange Inverse (ALEXI) data set [*Anderson et al*., 2007a,b]. The NTSG data set was eliminated due to its poor correlation with precipitation and runoff over the basin. The WM data set is used as the initial evapotranspiration estimate over the UBN basin since it had a better correlation with the precipitation data set. It should be mentioned that the ALEXI data set had the most consistent estimate of annual actual ET compared to (P-R) data over the basin. This data set was reserved to provide verification for the final data assimilation actual ET estimates.

4.1.5. Soil Moisture Data

Three water storage data sets were considered: the Climate Prediction Center (CPC) global monthly soil moisture data [*van den Dool et al*., 2003], the Gravity Recovery and Climate Experiment (GRACE) terrestrial water storage [*Chambers*, 2006], and the European Space Agency—Climate Change Initiative (ESA-CCI) soil moisture product [*Liu et al*., 2012]. A comparison between the long-term seasonal pattern of the terrestrial water storage anomalies and soil moisture data sets is shown in Figure 8. The GRACE and the CPC data sets agree very well. However, the ESA soil moisture shows the temporal distribution of the soil moisture for the top soil layer only. Thus the soil moisture range in the ESA data set is smaller than the other data sets and the peak soil moisture occurs earlier in July and August following the rainy season. The GRACE terrestrial water storage is used here as a measurement of the basin average soil water storage averaged over the basin since it is the most compatible with our vertically aggregated definition of water storage.

4.2. Constraint Inputs

The data needed for the optimization problem constraints can be summarized as follows:

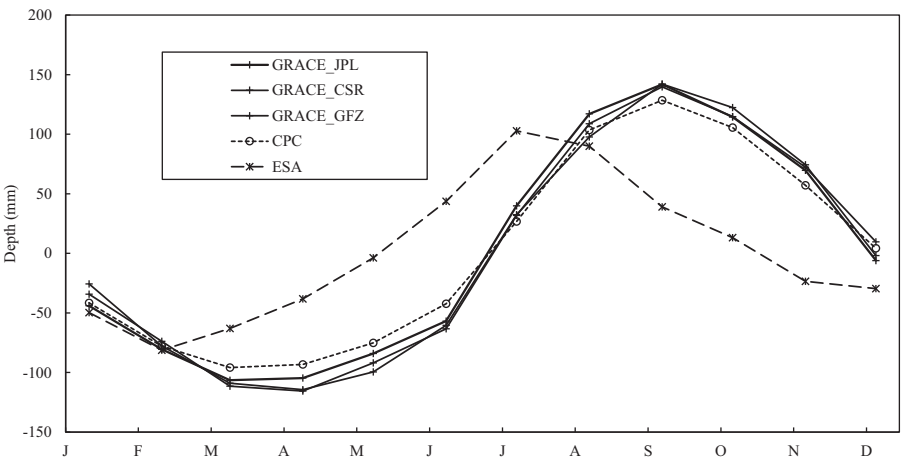

Figure 8. Comparison between the temporal distribution of GRACE and CPC anomaly water storage depth and ESA surface soil moisture data sets for the period 2002–2013.

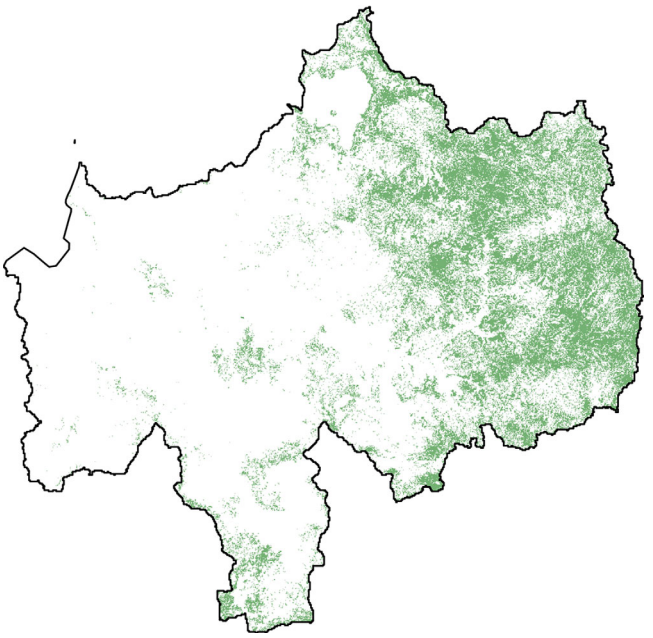

Figure 9. The croplands in the upper Blue Nile basin based on the MODIS 2009 land use data set.

4.2.1. Flow Direction Data

The information sources considered for determining flow directions were (1) the existing global data from the Dominant River Tracing (DRT) method [*Wu et al.*, 2011] or (2) the built in Arc Map flow direction calculator. Although both options give similar results, however, the DRT method was used since it has been compared with river directions and validated accordingly.

4.2.2. Soil Water Holding Capacity

The soil water holding capacity was obtained from the Harmonized World Soil Database (HWSD) which is a 30 arc-second raster database [*Nachtergaele*, 1999]. The HWSD soil water holding capacity map was upscaled by averaging values within our 0.25° pixels.

4.2.3. Crop Data

The crop areas were obtained from the updated Global Cropland and Pasture Data from 1700–2007. The cropped areas were updated using the 2009 Land cover MODIS data shown in Figure 9 [*Broxton et al.*, 2014]. The cropping pattern and crop area fractions for major crop groups used to generate the generalized crop factor for the UBN analysis were derived from the 1992 global cropland maps [*Ramankutty and Foley*, 1998]. The cropping pattern were compared to crop maps of the Atlas of Agricultural Statistics 2006/2007–2010/2011 produced by the Central Agency of Statistics (CSA) of the Federal Democratic Republic of Ethiopia (FDRE) and the International Food Policy Research Institute (IFPRI) and the cropping density was modified accordingly.

4.2.4. Radiation Data

The National Aeronautics and Space Administration (NASA) surface Radiation budget (SRB) data set [*Darnell et al.*, 1996; *Gupta et al.*, 1999] is used to calculate the monthly net radiation available over the UBN basin.

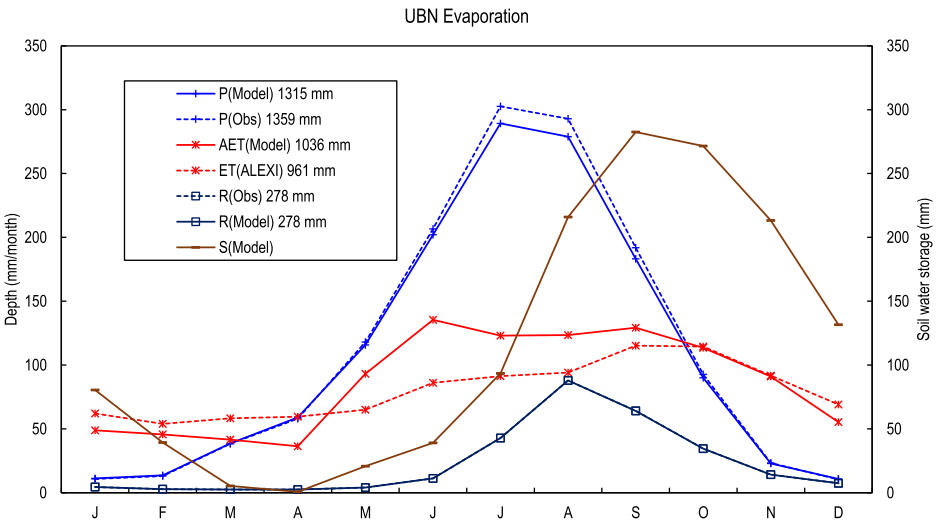

Figure 10. A summary of the temporal distribution of the UBN basin water buget depths: Precipitation (P), actual evapotranspiration (ET), basin runoff (R), and basin soil water storage (S). Shown is the mean annual cycle for the period 2002–2013.

Table 3. A Summary of the Long-Term Annual Water Budget Depths for Data Sets Used as Input to the Model and the Assimilated Water Budget Depths and the Percentage Change of the Assimilated Depth From the Initial Input Data for the Period (2002–2012)

Depth (mm)	Data	Estimate	% Change
Precipitation	1359	1315	3
Evapotranspiration	656	1036	58
Runoff	276	278	0.7

[a]The input data sets are: TRMM 3B43 v7 precipitation data, WM annual actual evapotranspiration data, and flow gauge measurements at Diem station. It should be noted that the initial input data have a closure error of 444 mm.

5. Results and Discussion

This paper describes the application of least-squares data assimilation methods to estimate rainfall, actual and potential evapotranspiration, soil storage, and river-flow over the data-scarce UBN basin. The spatially averaged assimilated estimates are shown in Figure 10. The assimilation model results suggest that TRMM precipitation data and the CRU PET data are about 12 percent larger than the least-square estimates. The estimated soil water storage and the runoff from the UBN basin agree with the observed values from GRACE and the flow gauge station measurements. The most important output of the data assimilation procedure is the actual evapotranspiration estimate which is estimated to be 1036 mm (Table 3). This estimate agrees with the global distribution of the annual-mean evaporation rate estimated by *Baumgartner and Reichel* [1975]. The assimilated actual evapotranspiration exceeds the potential evaporation during the June–October season. In the rainy season, the evaporation over the basin is energy limited due to the dense cloud cover. However during the rainy season, the natural vegetation and crops flourish which increases the surface roughness and enhances the transport of water vapor transportation near the surface and as a result the evaporation of intercepted rain occurs at rates higher than potential evaporation [*Shuttleworth*, 1988; *ElTahir and Bras*, 1994]. Table 4 shows a comparison between our model basin precipitation and runoff depth estimates and estimates by for the three seasons: the dry season ``Bega" (October–February), the

Table 4. A Comparison Between Our Model Estimate of the Seasonal UBN Basin Precipitation, Runoff Depths in mm and Runoff Coefficient (%) Depth Over the Period (2002–2012) and the Seasonal Observations of the UBN Basin Precipitation, Runoff Depths in mm and Runoff Coefficient (%) After *Tesemma et al*. [2010] for the period (1964–2003)

Season	P_{obs}	P_{Model}	R_{obs}	R_{Model}	RC_{obs}	RC_{Model}
Annual	1286	1315	268	278	21	21
Dry Season *(Bega: Oct–Feb)*	151	148	63	63	42	42.5
Short Rainy Season *(Belg: Mar–May)*	218	213	7	9	3.2	4.2
Long Rainy Season *(Kiremt: Jun–Sep)*	916	953	198	206	21.6	21.6

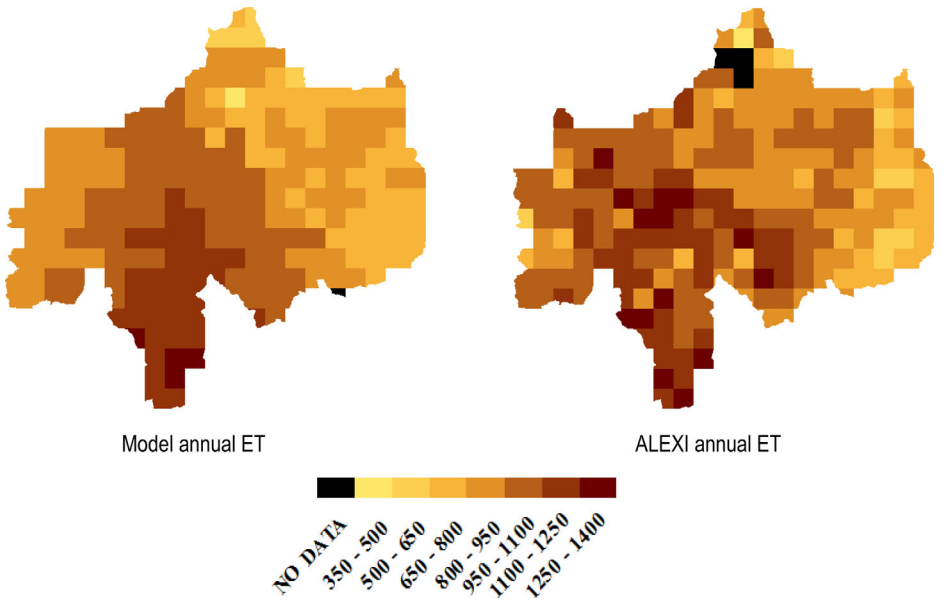

Figure 11. A comparison between the spatial distribution of the ALEXI and estimated long-term average annual ET depth over the UBN basin for the period 2002–2013.

Table 5. Summary of the Annual Water Budget Depths for Five Subbasins

Depth (mm)	BK	KK	KM	MD
Precipitation	1019	1189	1338	1302
Evapotranspiration	779	973	1098	931
Runoff	269	202	251	357
RC %	26	17	19	27

short rainy season ``Belg" (March–May), and the long-rainy season ``Kiremt" (June–September). The comparison shows that our model captures the seasonal variability in the precipitation and runoff and the runoff coefficient which is highest during the dry season and lowest during the short rainy season. This can be explained by the saturated soil moisture of the UBN basin soil at the end of the long-rainy season which enhances runoff during the dry season and dry basin soil at the end of the dry season significantly increases the infiltration losses during the short-rainy season.

A comparison between the ALEXI product and the estimated actual evapotranspiration is also shown in Figure 11. ALEXI is a two-source model that estimates the surface energy balance using Thermal infrared based observations of morning land surface temperatures (LST) rise acquired by geostationary satellites [*Anderson et al.*, 1997, 2007b]. Therefore, ALEXI evapotranspiration estimates are limited to clear-sky conditions when the surface is visible to the satellite sensor to measure LST. A cloud gap-filling algorithm was developed to improve the model output during cloudy conditions [*Anderson et al.*, 2007a]. However, over long cloudy periods which is the case during the rainy season over the UBN, basin ALEXI ET estimates retrievals still do not have continuous coverage because of missing observations. Therefore ALEXI may not yield accurate actual ET when clear-sky conditions do not apply. The comparison shows that ALEXI does a better job than the other data products in estimating the annual actual evapotranspiration from the basin since it has the least water budget closure error. However, ALEXI has a different spatial distribution over the basin and appears to underestimate evapotranspiration during the rainy season. Figure 11 shows the spatial distribution of the estimated and ALEXI annual evapotranspiration depths over the UBN basin. The data assimilation estimate has a smoother spatial distribution but both estimates agree to a large extent on the spatial distribution of the annual evapotranspiration depth. However, in the rainy season, they have different spatial distributions.

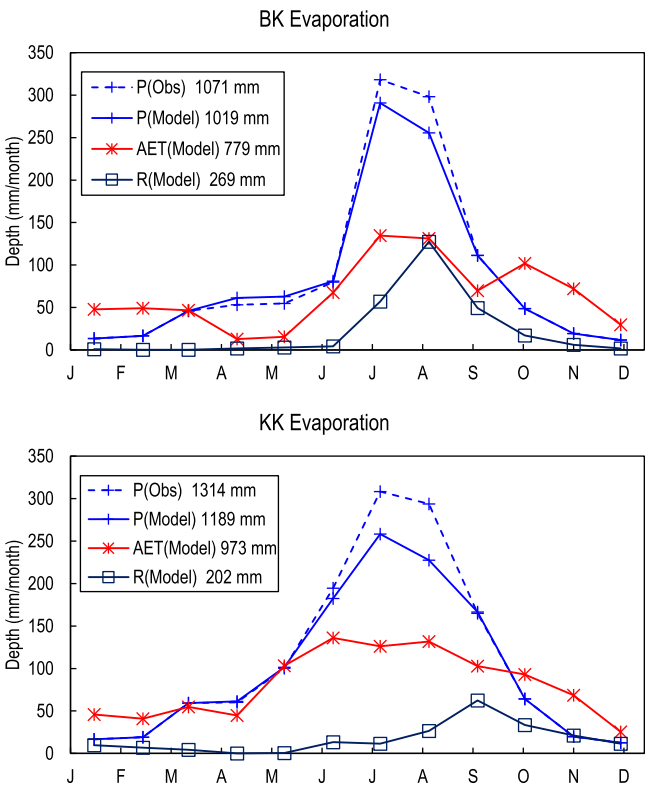

Figure 12. A summary of the temporal distribution of the BahirDar-Kessie and Kessie-Karadobi subbasins water buget depths: Precipitation (P), actual evapotranspiration (ET), basin runoff (R), and basin soil water storage (S). Shown is the mean annual cycle for the period 2002–2013.

In order to investigate the spatial evapotranspiration trends over the UBN basin, we divided the basin into four subbasins and estimated the incremental flows between the gauge stations. The subbasins are shown in Figure 8 and can be identified as: BahirDar-Kessie (BK) subbasin, Kessie-Karadobi (KK) subbasin, Karadobi-Mendaya (KM) subbasin, and Mendaya-Diem (MD) subbasin. A summary of the annual water budget depths of each of these subbasins is given in Table 5. The climatology is different in the four subbasins. For instance, the

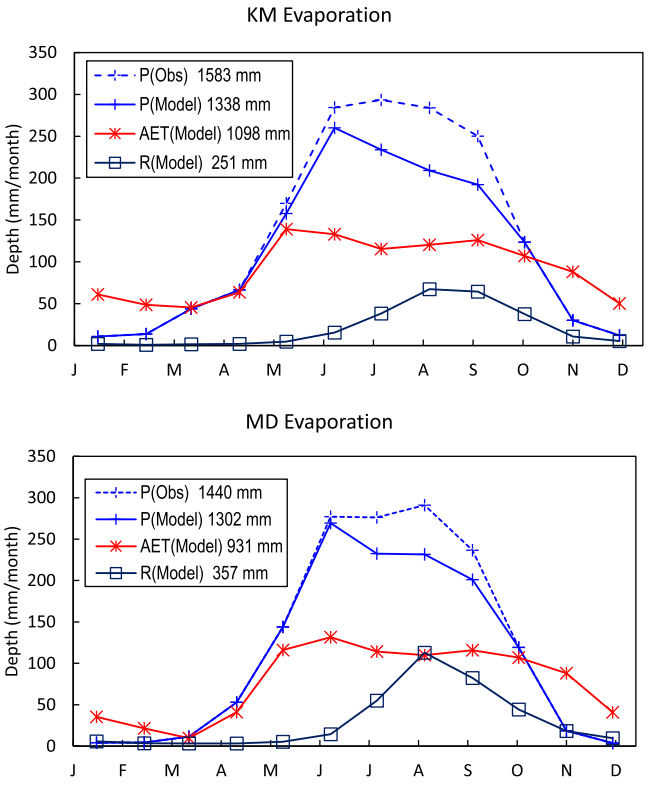

Figure 13. A summary of the temporal distribution of the Karadobi_Mendaya and Mendaya Diem subbasins water buget depths: Precipitation (P), actual evapotranspiration (ET), basin runoff (R), and basin soil water storage (S). Shown is the mean annual cycle for the period 2002–2013.

first and second wettest subbasins are KM and MD with annual precipitation depths of about 1338 and 1302 mm, respectively. The KM subbasin has the highest annual actual ET and consequently the lowest runoff coefficient. Figures 12 and 13 show the temporal distribution of selected hydrologic variables for the four subbasins. The actual ET over the KM basin exceeds the PET in the period May through November with a peak actual evapotranspiration rate of about 150 mm/month extending from July through September and then gradually decreases to about 60 mm/month in January. This temporal distribution reflects high vegetation transpiration during and after the rainy season. In contrast, the MD subbasin experiences a similar peak AET from July through September with the AET depth decreasing more rapidly at about 40 mm/month in January. This highlights the lower level of vegetation cover in this subbasin, leading to a higher run-off coefficient. The driest subbasin is BK with an annual precipitation depth of about 1019 mm as shown in Figure 13. However this subbasin has the highest runoff coefficient. The low actual evapotranspiration in this subbasin is largely due to its location in the eastern highlands of Ethiopia where temperatures are lower and there is less vegetation cover. We have also compared the spatial distribution of our model estimate of the actual evapotranspiration to

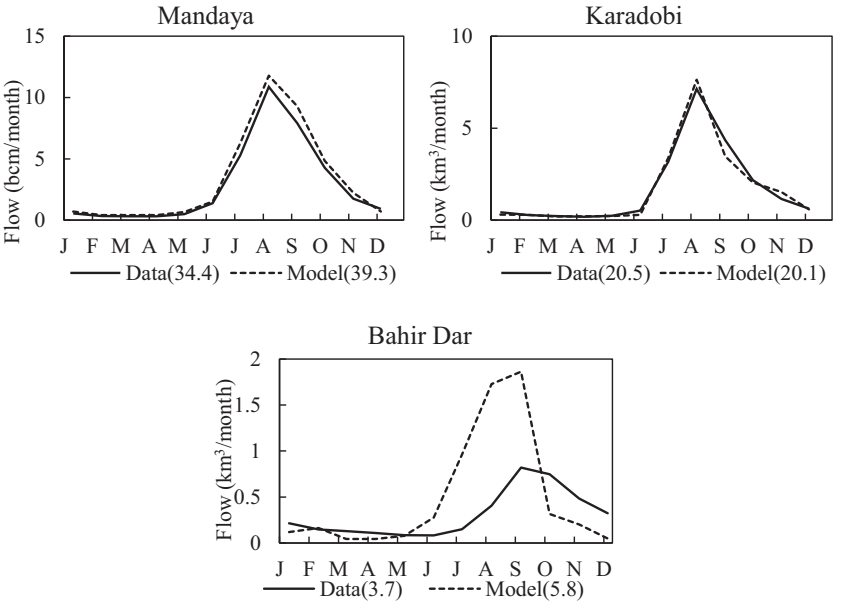

Figure 14. A comparison between the flow data at stations Mendaya, Karadobi, and Bahir Dar and the model flow routing at their locations when these input data are not given into the model.

precipitation (ET/P) ratio over the UBN basin for the period 2002–2013 to the basin land and the corresponding runoff coefficient as estimated by a recently published study by *Haregeweyn et al*., [2015]. Our estimates agree closely to the runoff coefficients estimated by this study where the eastern part of the basin is moderately and intensively cultivated with runoff coefficient varying between 20 and 25%, respectively [*Herweg and Stillhardt*, 1999; *Awulachew et al*.,2008; *Zenebe et al*.,2013] and the western part of the basin is mainly divided between traditional, Agrosilvicultural, and Silvipastoral land use with corresponding runoff coefficients of 12, 12, and 6%, respectively [*Geiger et al*.,1987; *California Department of Transportation*, 2006]. This agrees with our ET/P varying between 0.6 and 1.

It should be noted that the data available for Mendaya and Karadobi were found to be less reliable and given less weights since they are filled data generated from the river flow observations at Kessie and Diem. There was also a run where stations flow data were not given as inputs to the model to check how dependent the model to these data points is. Figure 14 shows a comparison between the flow data and the model pixel routed flow at the Karadobi, Mendaya, and BahirDar when the stations were hidden from the model. The comparison between the data and the model flows shows that the model is not highly dependent on Karadobi and Mendaya flow data since the change in the flow is less than 15%. On the other hand, the routing error at Lake Tana outlet (Bahir Dar) is high if the flow data were not assimilated into the model. This shows the high contribution of the flow stations around Lake Tana in improving the flow routing in the Tana subbasin and the reasoning behind the high concentration of stations around the Lake Tana basin.

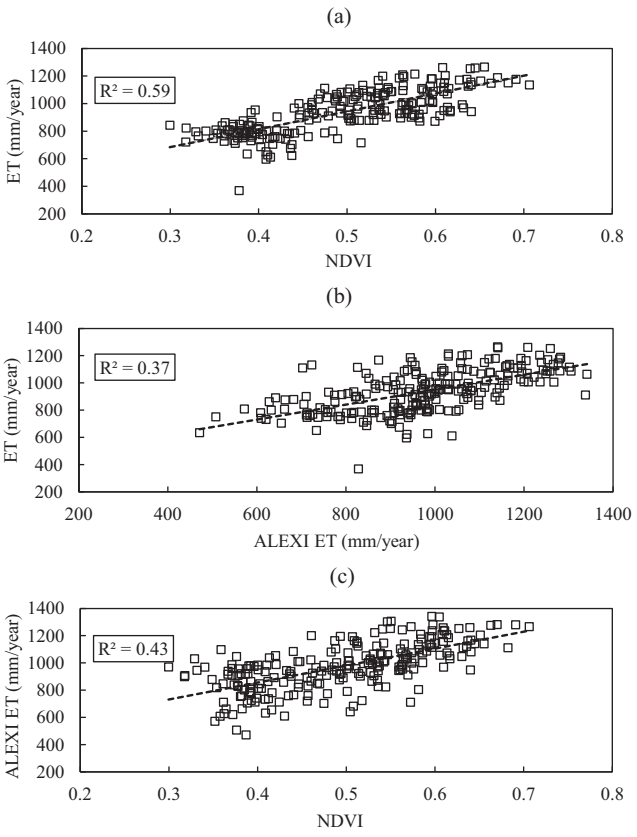

Figure 15. (a) The correlation between the data assimilated pixel long-term averaged annual actual evapotranspiration (ET) and the MODIS long-term averaged Normalized Difference Vegetation Index (NDVI) for the period 2002–2013. (b) The correlation between the data assimilated pixel long-term averaged annual actual evapotranspiration (ET) and the long-term averaged ALEXI annual actual evapotranspiration data set for the period 2002–2013. (c) The correlation between the pixel long-term averaged ALEXI annual actual evapotranspiration data set and the MODIS long-term averaged Normalized Difference Vegetation Index (NDVI) for the period 2002–2013.

For testing our estimates, we plotted our model estimates of actual evapotranspiration against the MODIS long-term average annual Normalized Difference Vegetation Index (NDVI) and the long-term average annual ALEXI actual evapotranspiration. The two products are completely independent from our analysis as shown in Figures 15a and 15b. Our model estimate is highly correlated with (NDVI) with a correlation coefficient of about 59% and has a lower correlation coefficient with the ALEXI data of about 37%. Figure 15c also shows the correlation between the long-term average ALEXI annual evapotranspiration and NDVI with a significantly lower correlation coefficient. In order to investigate the spatial variability of the annual evapotranspiration over the upper Blue Nile basin, a multivariate regression analysis was conducted with several variables such as precipitation, radiation, NDVI, soil properties, topography, and Temperature (see Table 6). It was found that precipitation, radiation, and NDVI collectively explain about 70% of the spatial variability in evapotranspiration over the UBN basin.

6. Conclusions

With the rapid population growth in Ethiopia, the demand for water is

Table 6. Summary of the Multivariate Regression Analysis of the Model Long-Term Average Evapotranspiration Estimate With the Long-Term Average Annual TRMM Precipitation Data, Long-Term Average Annual NASA-SRB Radiation Data, Long-Term Average Annual MODIS NDVI Data Set, AFSIS %S and Data Set and Slope Calculated Using SRTM Data for the Period (2002–2012)[a]

	P	NDVI	Rad	T	%Sand	%Slope	ET_{Model}
ET_{Model}	0.46	0.58	0.22	0.08	0.24	0.03	1
P, NDVI							0.60
P, Radf							0.52
P, Rad, NDVI							0.68
P, NDVI, Rad, %Sand							0.69
P, NDVI, Rad, %Sand, %Slope							0.7

[a]Shown is the coefficient of determination.

increasing and proper allocation of water resources is a critical step in developing the country. Evapotranspiration is a key component of the water budget. Three evapotranspiration data sets were examined over the UBN basin and they all underestimate the actual evapotranspiration and disagree about its temporal and spatial distributions. A better understanding of the temporal and spatial dynamics of the basin's hydrology is crucial to properly guide decision making and planning of hydropower and agricultural development. Previous studies have investigated the lumped hydrology of the basin but no study investigated the spatial distribution of evapotranspiration. In this paper, we have presented a framework for understanding the upper Blue Nile basin hydrology by integrating climatic, geographic, hydrologic, and agricultural data sets using a one-layer soil water budget model. This framework deals with data uncertainties and yields estimates that are consistent with the principles of mass and energy conservation while also fitting available observations as closely as possible. Our data assimilation procedure estimates the annual evapotranspiration from the upper Blue Nile basin to be about 1036 mm which is about 380 mm higher than the other readily available data sets examined in this paper. We identified spatial trends of evaporation by dividing the basin into subbasins. We observed that temperature and vegetation type play important roles in shaping the evapotranspiration and runoff from the basin. This analysis can be extended to examine the interannual variability of the basin's hydrology and to obtain consistent estimates of precipitation, evapotranspiration, and runoff time series data. Moreover, the data assimilation framework described here can be easily applied to other basins with limited data availability.

Acknowledgment
All the spatial data used in this research are available freely as stated in the Data section. This work was funded by the Cooperative Agreement between the Masdar Institute of Science and Technology (Masdar Institute), Abu Dhabi, UAE and the Massachusetts Institute of Technology (MIT), Cambridge, MA, USA - Reference 02/MI/MIT/CP/11/07633/GEN/G/00.

References

Adler, R. F., et al. (2003), The Version 2 Global Precipitation Climatology Project (GPCP) monthly precipitation analysis (1979-Present), *J. Hydrometeorol.*, *4*, 1147–1167.

Anderson, M. C., J. M. Norman, G. R. Diak, W. P. Kustas, and J. R. Mecikalski (1997), A two-source time-integrated model for estimating surface fluxes using thermal infrared remote sensing, *Remote Sens. Environ.*, *60*, 195–216.

Anderson, M. C., J. M. Norman, J. R. Mecikalski, J. P. Otkin, and W. P. Kustas (2007a), A climatological study of evapotranspiration and moisture stress across the continental U.S. based on thermal remote sensing: I. Model formulation, *J. Geophys. Res.*, *112*, D10117, doi:10.1029/2006JD007506.

Anderson, M. C., J. M. Norman, J. R. Mecikalski, J. P. Otkin, and W. P. Kustas (2007b), A climatological study of evapotranspiration and moisture stress across the continental U.S. based on thermal remote sensing: II. Surface moisture climatology, *J. Geophys. Res.*, *112*, D11112, doi:10.1029/2006JD007507.

Awulachew, S. B., M. Mccartney, T. S. Steenhuis, and A. A. Ahmed (2008), *A Review of Hydrology, Sediment and Water Resource Use in the Blue Nile Basin*, *IWMI Working Pap. 131*, p. 87, Int. Water Manage. Inst., Colombo, Sri Lanka.

Baumgartner, A., and E. Reichel (1975), *The World Water Balance*, Elsevier, N. Y.

Broxton, P. D., X. Zeng, D. Sulla-Menashe, and P. A. Troch (2014a), A global land cover climatology using MODIS Data, *J. Appl. Meteorol. Climatol.*, *53*, 1593–1605, doi:10.1175/JAMC-D-13-0270.1.

California Department of Transportation (2006), *Highway Design Manual: Hydrology 8101-25*. [Available at http://www.dot.ca.gov/hq/oppd/hdm/pdf/chp0810.pdf.]

Collick, A. S., Z. M. Easton, T. Ashagrie, B. Biruk, S. Tilahun, E. Adgo, S. B. Awulachew, G. Zeleke, and T. S. Steenhuis (2009), A simple semi-distributed water balance model for the Ethiopian Highlands, *Hydrol. Processes*, *23*, 3718–3727.

Conway, D. (1997), A water balance model of the Upper Blue Nile in Ethiopia, *Hydrol. Sci. J.*, *42*(2), 265–286, doi:10.1080/02626669709492024.

Conway, D. (2000), The climate and hydrology of the upper Blue Nile River, *Geogr. J.*, *166*, 49–62, doi:10.1111/j.1475-4959.2000.tb00006.x.

Chambers, D. P. (2006), Evaluation of new GRACE time-variable gravity data over the ocean, *Geophys. Res. Lett.*, *33*, L17603, doi:10.1029/2006GL027296.

Darnell, W. L., W. F. Staylor, N. A. Ritchey, S. K. Gupta, and A. C. Wilber (1996), New data set on surface radiation budget, *Eos Trans. AGU*, *77*(9), 86–86.

Decker, M., M. Brunke, Z. Wang, K. Sakaguchi, X. Zeng, and M. Bosilovich (2012), Evaluation of the reanalysis products from GSFC, NCEP, and ECMWF using flux tower observations, *J. Clim.*, *25*, 1916–1944, doi:10.1175/JCLI-D-11-00004.1.

Eltahir, E. A. B. (1996), ElNino and the natural variability in the flow of the Nile River, *Water Resour. Res.*, *32*, 131–137.
Eltahir, E. A., and R. L. Bras (1994) Precipitation recycling in the Amazon basin, *Q. J. R. Meteorol. Soc.*, *120*(518), 861–880.
Food and Agriculture Organization of the United Nations FAO/IIASA/ISRIC/ISS-CAS/JRC (2012), *Harmonized World Soil Database*, version 1.2, Rome, IIASA, FAO/Laxenburg.
Gao, H., Q. Tang, C. R. Ferguson, E. F. Wood, and D. P. Lettenmaier (2010), Estimating the water budget of major US river basins via remote sensing, *Int. J. Remote Sens.*, *31*(14), 3955–3978.
Geiger, W. F., J. Marsalek, W. J. Rawls, and F. C. Zuidema (1987*), Manual on Drainage in Urbanized Areas, Vol. 1, Planning and Design of Drainage Systems, Stud. Rep. Hydrol.*, The United Nations Educational, Scientific and Cultural Organization, Paris.
Gupta, S. K., N. A. Ritchey, A. C. Wilber, C. H. Whitlovk, G. G. Gibson, and P. W. Stackhouse Jr. (1999), A climatology of surface radiation budget derived from satellite data, *J. Clim.*, *12*, 2691–2710.
Haregeweyn, N., A. Tsunekawa, M. Tsubo, D. Meshesha, and E. Adgo (2015), Modeling the hydrologic effects of land and water development interventions: A case study of the upper Blue Nile river basin, *Reg. Environ. Change*, *15*, 1–16, doi:10.1007/s10113-015-0813-2.
Herweg, K., and B. Stillhardt (1999), The variability of soil erosion in the highlands of Ethiopia and Eritrea, Soil conservation research project, *Res. Rep. 42*, Cent. for Dev. and Environ., Univ. of Berne, Berne.
Houser, P. R., W. J. Shuttleworth, J. S. Famiglietti, H. V. Gupta, K. H. Syed, and D. C. Goodrich (1998), Integration of soil moisture remote sensing and hydrologic modeling using data assimilation, *Water Resour. Res.*, *34*, 3405–3420.
Huffman, G. J., D. T. Bolvin, E. J. Nelkin, D. B. Wolff, R. F. Adler, G. Gu, Y. Hong, K. P. Bowman, and E. F. Stocker (2007), The TRMM Multisatellite Precipitation Analysis (TMPA): Quasi-global, multiyear, combined-sensor precipitation estimates at fine scales, *J. Hydrometeorol.*, *8*, 38–55.
Kanamitsu, M., W. Ebisuzaki, J. Woollen, S.-K. Yang, J. J. Hnilo, M. Fiorino, and G. L. Potter (2002), NCEP-DOE AMIP-II reanalysis (R-2), *Bull. Am. Meteorol. Soc.*, *83*(11), 1631–1643.
Kim, U., J. J. Kaluarachchi, and V. U. Smakhtin (2008), Generation of monthly precipitation under climate change for the upper Blue Nile river basin, Ethiopia, *J. Am. Water Resour. Assoc.*, *44*, 1231–1247, doi:10.1111/j.1752-1688.2008.00220.x.
Leff, B., N. Ramankutty, and J. A. Foley (2004), Geographic distribution of major crops across the world, *Global Biogeochem. Cycles*, *18*, GB1009, doi:10.1029/2003GB002108.
Liu, Y. Y., W. A. Dorigo, R. M. Parinussa, R. A. M. de Jeu, W. Wagner, M. F. McCabe, J. P. Evans, and A. I. J. M. van Dijk (2012), Trend-preserving blending of passive and active microwave soil moisture retrievals, *Remote Sens. Environ.*, *123*, 280–297.
Markowitz, H. (1956), The optimization of a quadratic function subject to linear constraints, *Nav. Res. Log.*, *3*, 111–133, doi:10.1002/nav.3800030110.
McLaughlin, D. (1995), Recent developments in hydrologic data assimilation, *Rev. Geophys.*, *33*, 977–984.
Mitchell, T. D., and P. D. Jones (2005), An improved method of constructing a database of monthly climate observations and associated high-resolution grids, *Int. J. Climatol.*, *25*, 693–712.
Nachtergaele, F. O. (1999), From the soil map of the world to the digital global soil and terrain database: 1960–2002, in *Handbook of Soil Science*, edited by M. E. Sumner, pp. 5–17, CRC Press, Boca Raton, Fla.
Onogi, K., H. Koide, M. Sakamoto, S. Kobayashi, J. Tsutsui, H. Hatsushika, and K. Wada (2005), JRA-25: Japanese 25-year re-analysis project—progress and status, *Q. J. R. Meteorol. Soc.*, *131*(613), 3259–3268.
Onogi, K., J. Tsutsui, H. Koide, M. Sakamoto, S. Kobayashi, H. Hatsushika, and R. Taira (2007), The JRA-25 reanalysis, *J. Meteorol. Soc. Japan*, *85*(3), 369–432.
Pan, M., and E. F. Wood (2006), Data assimilation for estimating the terrestrial water budget using a constrained ensemble Kalman filter, *J. Hydrometeorol.*, *7*(3), 534–547.
Pan, M., A. K. Sahoo, T. J. Troy, R. K. Vinukollu, J. Sheffield, and E. F. Wood (2012), Multisource estimation of long-term terrestrial water budget for major global river basins, *J. Clim.*, *25*(9), 3191–3206.
Ramankutty, N., and J. A. Foley (1998), Characterizing patterns of global land use: An analysis of global croplands data, *Global Biogeochem. Cycles*, *12*, 667–685.
Ramankutty, N., and J. A. Foley (1999), Estimating historical changes in global land cover: Croplands from 1700 to 1992, *Global Biogeochem. Cycles*, *13*, 997–1027.
Rienecker, M. M., M. J. Suarez, R. Gelaro, R. Todling, J. Bacmeister, E. Liu, and J. Woollen (2011), MERRA: NASA's modern-era retrospective analysis for research and applications, *J. Clim.*, *24*(14), 3624–3648.
Saha, S., et al. (2010), The NCEP climate forecast system reanalysis, *Bull. Am. Meteorol. Soc.*, *91*(8), 1015–1057.
Sahoo, K. K., A. K. Tripathi, A. Pareek, S. K. Sopory, and S. L. Singla-Pareek (2011), An improved protocol for efficient transformation and regeneration of diverse indica rice cultivars, *Plant Methods*, *7*, 49, doi:10.1186/1746-4811-7-49.
Sheffield, J., C. R. Ferguson, T. J. Troy, E. F. Wood, and M. F. McCabe (2009), Closing the terrestrial water budget from satellite remote sensing, *Geophys. Res. Lett.*, *36*, L07403, doi:10.1029/2009GL037338.
Shuttleworth, W. J. (1988), Evaporation from Amazonian rainforest, *Philos. Trans. R. Soc. London, B*, *233*, 321–346.
Siam, M. S., and E. A. B. Eltahir (2015), Explaining and forecasting interannual variability in the flow of the Nile River, *Hydrol. Earth Syst. Sci.*, *19*(3), 1181–1192.
Siam, M. S., M. Demory, and E. A. B. Eltahir (2013), Hydrological cycles over the Congo and upper blue Nile basins: Evaluation of general circulation model simulations and reanalysis products, *J. Clim.*, *26*, 8881–8894, doi:10.1175/JCLI-D-12-00404.1.
Siam, M. S., G. Wang, M. E. Estelle, and E. A. B. Eltahir (2014), Role of the Indian Ocean sea surface temperature in shaping natural variability in the flow of the Nile River, *Clim. Dyn.*, *43*, 1011–1023.
Simmons, A. J., S. Uppala, D. Dee, and S. Kobayashi (2007), ERA-Interim: New ECMWF reanalysis products from 1989 onwards, *ECMWF Newsl.*, 110, pp. 25–35, ECMWF, Reading, U. K.
Tafesse, T. (2001), The hydropolitical assessment of the Nile question: An Ethiopian perspective, *Water Int.*, *26*(4), 1–11, doi:10.1080/02508060108686945.
Tekleab, S., S. Uhlenbrook, Y. Mohamed, H. H. G. Savenije, M. Temesgen, and J. Wenninger (2011), Water balance modeling of Upper Blue Nile catchments using a top-down approach, *Hydrol. Earth Syst. Sci.*, *15*, 2179–2193, doi:10.5194/hess-15-2179-2011.
Tesemma, Z. K., Y. A. Mohamed, and T. S. Steenhuis (2010), Trends in rainfall and runoff in the Blue Nile Basin: 1964-2003, *Hydrol. Processes*, *2424*, 3747–3758.
Uppala, S. M., et al. (2005), The ERA-40 re-analysis, *Q. J. R. Meteorol. Soc.*, *131*(612), 2961–3012.
Uppala, S., D. Dee, S. Kobayashi, P. Berrisford, and A. Simmons (2008), Towards a climate data assimilation system: Status update of ERA-Interim, *ECMWF Newsl.*, *115*, 12–18.

van den Dool, H., J. Huang, and F. Yun (2003), Performance and analysis of the constructed analogue method applied to U.S. soil moisture over 1981–2001, *J. Geophys. Res.*, *108*(D16), 8617, doi:10.1029/2002JD003114.

Willmott, C. J., and K. Matsuura (2000), Monthly terrestrial water budget climatologies data set. [Available online at http://climate.geog.udel.edu/~climate/html_pages/download.html.]

Wu, H., J. S. Kimball, N. Mantua, and J. Stanford (2011), Automated upscaling of river networks for macroscale hydrological modeling, *Water Resour. Res.*, *47*, W03517, doi:10.1029/2009WR008871.

Zenebe, A., M. Vanmaercke, J. Poesen, G. Verstraeten, N. Haregeweyn, M. Haile, K. Amare, J. Deckers, and J. Nyssen (2013), Spatial and temporal variability of river flows in the degraded semi-arid tropical mountains of northern Ethiopia, *Z. Geomorphol.*, *57*(2), 143–169.

Zhang, K., J. S. Kimball, Q. Mu, L. A. Jones, S. J. Goetz, and S. W. Running (2009), Satellite based analysis of northern ET trends and associated changes in the regional water balance from 1983 to 2005 (2009), *J. Hydrol.*, *379*, 92–110, doi:10.1016/j.jhydrol.2009.09.047.

Zhang, K., J. S. Kimball, R. R. Nemani, and S. W. Running (2010), A continuous satellite-derived global record of land surface evapotranspiration from 1983-2006, *Water Resour. Res.*, *46*, W09522, doi:10.1029/2009WR008800.